

Dielectric Boundary Forces in Numerical Poisson-Boltzmann Methods:

Theory and Numerical Strategies

Xiang Ye,¹ Jun Wang,¹ and Ray Luo^{1,2}

1. Department of Molecular Biology and Biochemistry

University of California, Irvine, CA 92697, USA

2. Department of Biomedical Engineering

University of California, Irvine, CA 92697, USA

Continuum modeling of electrostatic interactions based upon numerical solutions of the Poisson-Boltzmann equation has been widely adopted in biomolecular applications. To extend their applications to molecular dynamics and energy minimization, robust and efficient methodologies to compute solvation forces must be developed. In this study, we have first reviewed the theory for the computation of solvation forces, especially for the computation of dielectric boundary forces, based on the definition of Maxwell stress tensor. This is followed with further theoretical analysis to derive a new formulation suitable for the finite-difference Poisson-Boltzmann numerical methods. Additional numerical enhancements are then proposed within the new formulation. We have validated the new formulation with idealized analytical systems and realistic molecular systems. Our analyses show that the new formulation converges better and are numerically more stable than the existing method for the tested systems.

I. Introduction

Solvation interaction is one of the essential determinants of the structure and function of proteins and nucleic acids.¹⁻¹⁴ It has been shown that continuum electrostatics represents an effective and physically sound approach which makes it possible to account for a number of phenomena involving solvent electrostatic effects on the function of biological macromolecules.¹⁻¹⁴ Due to the availability of high performance computing resources, continuum modeling of electrostatic interactions, which is based upon numerical solutions of the Poisson-Boltzmann equation (PBE), has been widely adopted in biomolecular applications.¹⁻¹⁴ Among the numerical solution methods for PBE, finite difference methods (FDM),¹⁵⁻³² finite element methods (FEM),³³⁻³⁹ and boundary element methods (BEM)⁴⁰⁻⁵⁴ are mostly used.

A disadvantage of the numerical continuum electrostatics methods is that it is conceptually difficult to incorporate them into molecular mechanics algorithms, mainly because of the problem of assigning solvation forces.^{26, 34, 41, 55-62} Along with other limitations, the PBE is mostly solved for static conformations of biomolecules in practical applications. To extend the application of the PBE to molecular dynamics and energy minimization, robust and efficient methodologies to compute solvation forces must be developed. It has been shown that solvation forces can be divided into two components: reaction field forces and dielectric boundary forces.^{26, 34, 41, 55-62} Reaction field forces are straightforward to compute, but computation of dielectric boundary forces (*DBF*) remains as a challenge in the widely used classical two-dielectric model that has been successfully in a wide range of biomolecular applications.¹⁻¹⁴

The challenge can be appreciated by noting that the derivative of dielectric constant at the dielectric interface between solvent and solute, where DBF is located, is infinite in the classical two-dielectric model. There have been several proposals in the past to bypass the “dielectric singularity” completely via the use of smoothed dielectric transition models.^{26, 61} When doing so we need to bear in mind that the dielectric transition layer cannot be set to an arbitrary thickness and still hope for realistic representations of solvation interactions. The upper bound of the thickness may, in principle, set a lower bound on the discretization resolution* if we insist upon the quality of the smoothed dielectric models.

Many efforts have been invested to calculate the DBF .^{26, 55-56, 59, 62} The “virtual work” method is, in a sense, the most definitive.⁵⁵ In the “virtual work” method the electrostatic energy G is recalculated for small displacements d of each atom in the x , y , and z directions, respectively. The force is then just $-\Delta G/d$ for each direction. The limitation of this approach, however, is that at least four full numerical calculations are required in order to calculate each force vector. Apparently, this is only realistic for molecules treated as rigid bodies.

Davis and McCammon proposed a DBF formulation by examining the integration of the Maxwell stress tensor for the classical two-dielectric model. The DBF surface density was shown as⁵⁵

$$\mathbf{f}_{DBF} = \frac{1}{4\pi}(\varepsilon_o - \varepsilon_i)(\mathbf{E}_o \cdot \mathbf{E}_i)\hat{\mathbf{n}}, \quad (1)$$

where ε_o and ε_i are the dielectric constants of the solvent and the solute, respectively, and \mathbf{E}_o and \mathbf{E}_i are the values of the electric field evaluated on the solvent and solute sides of

* For example, the dielectric transition layer has to be covered by a few grid points in the widely used FDM solutions to guarantee accuracy and numerical stability during simulations.

the molecular surface, respectively. Note that the use of eqn (1) is difficult for the FDM solutions because the grid potentials are least accurate close to the solute/solvent dielectric interface.^{16,29,53} In addition, it requires a numerical surface integration that can be very expensive within the FDM. Recently Che *et al.* revisited the *DBF* calculation through a variational strategy in the classical two-dielectric model.⁶² Given the assumption that the normal surface field contributes predominantly to *DBF*, they showed that the *DBF* could be formulated as

$$\mathbf{f}_{DBF} = \frac{1}{8\pi} \left(\frac{1}{\epsilon_i} - \frac{1}{\epsilon_o} \right) |\epsilon \nabla \phi|^2 \hat{\mathbf{n}} \quad (2)$$

where $\epsilon \nabla \phi$ represents the continuous normal dielectric displacement vector on the solute/solvent dielectric interface.

The BEM is another promising approach to incorporate the continuum electrostatics into molecular mechanics simulations.^{41, 44, 63-67} The *DBF* calculation in the BEM using a polarization charge method was first described by Zauhar,⁵⁶ who showed that the *DBF* surface density can be calculated as

$$\mathbf{f}_{DBF} = \left[2\pi\sigma^2\epsilon_i + \frac{1}{8\pi}(\epsilon_o - \epsilon_i)|\mathbf{E}_o|^2 \right] \hat{\mathbf{n}}, \quad (3)$$

where σ is the surface polarization charge density. This expression was derived from eqn (1). The use of surface polarization charge density makes it straightforward in certain types of BEM where the Poisson's equation can be solved through the iteration of the surface polarization charge density. Cortis *et al.* also tried to compute the *DBF* via the Maxwell stress tensor for their FEM leading to the same formulation as that of Zauhar.³⁴

Gilson *et al.* presented a variational approach for the *DBF*,⁵⁹ and it was further tailored

into a numerical algorithm for the FDM. Their expression for the *DBF* volume density can be expressed as

$$\mathbf{g}_{DBF} = -\frac{1}{8\pi} |\mathbf{E}|^2 \nabla \varepsilon, \quad (4)$$

where ε is the dielectric constant and \mathbf{E} is the electric field. Note that the direction of the *DBF* in eqn (4) is consistent with that in eqn (1) and in its equivalent formulations because the gradient of dielectric transition is in the normal direction. Im *et al.* proposed a method equivalent to eqn (4) as²⁶

$$\mathbf{g}_{DBF} = \left[\frac{1}{8\pi} \phi \nabla \cdot \left(\frac{\partial \varepsilon}{\partial r} \nabla \phi \right) \right] \hat{\mathbf{n}} \quad (5)$$

where ϕ is the total electrostatic potential, r represents the atomic coordinates. Apparently both eqn (4) and (5) require smoothly varying dielectric models since $\nabla \varepsilon$ has to be finite, *i.e.* ε has to be designed to change from ε_i to ε_o sufficiently smoothly for stable numerical performance.⁶¹ This would exclude the classical two-dielectric model where $\nabla \varepsilon$ is infinite. Even if the harmonic average is used at the solute/solvent dielectric interface, direct numerical calculation of $\nabla \varepsilon$ is still unstable in molecular dynamics. This leads to large and unstable *DBF* that does not satisfy the “virtual work” principle. Numerical approximation of $\nabla \varepsilon$ may alleviate the problem, but instability cannot be completely eliminated in molecular dynamics.^{59, 68}

Even with these pioneer developmental efforts, the *DBF* calculation remains to be a bottleneck that limits the wide application of numerical PB methods in molecular simulations. Nevertheless, these prior efforts lay down the foundation for us to develop more accurate and robust methods. In this study, we intend to resolve the challenge within the widely used classical two-dielectric framework.¹⁻¹⁴ In the following we first review the theory for the

DBF calculation based on the Maxwell stress tensor. This is followed by the development of a new algorithm particularly designed for the FDM solutions. The performance of the new algorithm is then analyzed in detail and is compared with the well-established Gilson *et al.* method.⁵⁹

II. Methods

A. Theory

It is well known that the electrostatic force volume density (\mathbf{g}) can be derived through the divergence of the Maxwell stress tensor (\mathbf{P}) as⁶⁹

$$\begin{aligned}\mathbf{g} &= \nabla \cdot \mathbf{P} = \frac{\partial}{\partial x}(\hat{\mathbf{i}} \cdot \mathbf{P}) + \frac{\partial}{\partial y}(\hat{\mathbf{j}} \cdot \mathbf{P}) + \frac{\partial}{\partial z}(\hat{\mathbf{k}} \cdot \mathbf{P}) \\ &= \rho^f \mathbf{E} - \frac{1}{8\pi} |\mathbf{E}|^2 \nabla \varepsilon - \Delta \Pi \nabla \lambda\end{aligned}\quad (6)$$

where ρ^f is the fixed charge density, \mathbf{E} is the electric field, ε is the dielectric constant, and $\Delta \Pi$ is the excess osmotic pressure,⁷⁰ λ is the Stern layer defined so that it is 1 in regions accessible to the mobile ions and 0 elsewhere. This is consistent with the formulation of Gilson *et al.*⁵⁹ derived from the variation of the total electrostatic free energy.^{65,66} The force volume density that is responsible for the *DBF* can be rewritten as

$$\mathbf{g}_{DBF} = -\frac{1}{8\pi} |\mathbf{E}|^2 \nabla \varepsilon. \quad (7)$$

To remove the potential numerical instability in $\nabla \varepsilon$ and develop a new formulation that is more suitable for the FDM, we utilize a revised PBE. In the vicinity of the dielectric boundary $\rho^f = 0$, we have

$$\nabla \cdot (\varepsilon \mathbf{E}) = 0 \quad (8)$$

Differentiation by parts on the left hand side of eqn (8) gives

$$\nabla \varepsilon \cdot \mathbf{E} + \varepsilon \nabla \cdot \mathbf{E} = 0 \quad (9)$$

The second term of eqn (9) can be rewritten as

$$\varepsilon \nabla \cdot \mathbf{E} = \varepsilon \nabla \cdot (\mathbf{E}_c + \mathbf{E}_{RF}), \quad (10)$$

where \mathbf{E}_c is the Coulomb field and \mathbf{E}_{RF} is the reaction field. Since $\nabla \cdot \mathbf{E}_c = 4\pi\rho^f = 0$ in the vicinity of the dielectric boundary, eqn (10) can be simplified as

$$\varepsilon \nabla \cdot \mathbf{E} = \varepsilon \nabla \cdot \mathbf{E}_{RF} = 4\pi\varepsilon\rho^{pol}, \quad (11)$$

where $\rho^{pol} = \frac{1}{4\pi} \nabla \cdot \mathbf{E}_{RF}$ is the polarization charge density at the dielectric boundary. With eqn (9) and (11), $\nabla \varepsilon \cdot \mathbf{E}$ can be written as

$$\nabla \varepsilon \cdot \mathbf{E} = -\varepsilon \nabla \cdot \mathbf{E} = -4\pi\varepsilon\rho^{pol}. \quad (12)$$

To utilize the above conclusion to eqn (7), we first transform eqn (7) via a dot-product by \mathbf{E} on both sides

$$\mathbf{g}_{DBF} \cdot \mathbf{E} = -\frac{1}{8\pi} |\mathbf{E}|^2 \nabla \varepsilon \cdot \mathbf{E} = \frac{1}{2} \varepsilon \rho^{pol} |\mathbf{E}|^2. \quad (13)$$

Since the direction of \mathbf{g}_{DBF} follows the gradient of the dielectric constant, *i.e.* the normal direction of the surface ($\hat{\mathbf{n}}$), the left hand side of eqn (13) can further be transformed as

$$\mathbf{g}_{DBF} \cdot \mathbf{E} = g_{DBF} \hat{\mathbf{n}} \cdot \mathbf{E} = g_{DBF} E_n, \quad (14)$$

where is E_n the normal component of the surface field. Therefore

$$g_{DBF} = \frac{\mathbf{g}_{DBF} \cdot \mathbf{E}}{E_n} = \frac{\frac{1}{2} \varepsilon \rho^{pol} |\mathbf{E}|^2}{\mathbf{E} \cdot \hat{\mathbf{n}}}. \quad (15)$$

Thus \mathbf{g}_{DBF} can finally be written as

$$\mathbf{g}_{DBF} = g_{DBF} \hat{\mathbf{n}} = \frac{1}{2} \rho^{pol} \frac{\varepsilon |\mathbf{E}|^2}{E_n} \hat{\mathbf{n}} = \frac{1}{2} \rho^{pol} \frac{\varepsilon |\mathbf{E}|^2}{\mathbf{E} \cdot \hat{\mathbf{n}}} \hat{\mathbf{n}}. \quad (16)$$

There are several equivalent forms of eqn (16) by noting that $\mathbf{D} = \varepsilon \mathbf{E}$ and $D_n = \varepsilon E_n$:

$$\mathbf{g}_{DBF} = \frac{1}{2} \rho^{pol} \frac{\mathbf{D} \cdot \mathbf{E}}{E_n} \hat{\mathbf{n}} = \frac{1}{2} \rho^{pol} \frac{|\mathbf{D}|^2}{D_n} \hat{\mathbf{n}}. \quad (17)$$

These equivalent forms can be used to develop other alternative numerical strategies or approximations as will be shown in our later publications.

B. Numerical algorithm

In the FDM, the polarization charges can be regarded as being located at the dielectric boundary grid points.²⁹ It will be shown below that the grid-based polarization charges are very good numerical representations of the dielectric interface polarization charges and converge very well. Their errors are particularly small when typical grid spacings, i.e. 0.25 ~ 0.50 Å, are used. Given this numerical representation of polarization charges and eqn (16), the total *DBF* in the solution system, \mathbf{G}_{DBF} , can be computed numerically as

$$\mathbf{G}_{DBF} = \int \mathbf{g}_{DBF} dV \approx \frac{1}{2} \sum_{i=1}^{nbnd} q_i^{pol} \frac{\epsilon |\mathbf{E}_i|^2}{E_{n,i}} \hat{\mathbf{n}}_i, \quad (18)$$

where *nbnd* is the number of the solute/solvent dielectric boundary grid points where the polarization charges are located.[†] q_i^{pol} , \mathbf{E}_i , $E_{n,i}$, and $\hat{\mathbf{n}}_i$ are, respectively, the polarization charge, surface field, normal surface field, and surface normal unit vector at dielectric boundary grid point *i*. To further improve the numerical behavior of eqn (18), the polarization charges are projected to the analytical molecular surface as in the calculation of reaction field energy and forces with the polarization charges.²⁹ This reduces the grid-dependence of eqn (18) and the numerical uncertainty of the *DBF*. Of course it also improves the convergence of *DBF*. As will be discussed below, there is more room to further improve the numerical behavior of eqn (18).

C. Surface field calculation

[†] Of course the polarization charges are zero on all other grid points where there is no dielectric variation.

Use of eqn (18) needs electric field at the projection points of the polarization charges on the molecular surface. However, a practical question is which side of the molecular surface, *i.e.* the solute side or the solvent side, the surface field shall be interpolated when the polarization charges are projected onto the molecular surface. Apparently, the problem does not exist if the polarization charges stay on the grid points, which are rarely exactly located on the molecular surface. This turns out to be not a problem at least in theory because there is no preferred side in eqn (16), *i.e.* either side should work in theory. However, this does not mean that the numerical behavior is the same between the two approaches. Indeed, interpolations from the solute side and the solvent side are only highly consistent only when a very fine grid spacing is used, for example, 1/16 Å. At coarse grid spacing, interpolation from the solvent side turns out to be too noisy because of the much-reduced magnitude in electric field from solvent screening. Thus, surface field was interpolated from the solute side in the following numerical procedure.

We utilized the one-sided least-square interpolation method⁷¹ to obtain the surface potential and field at an arbitrary position (x_0, y_0, z_0) . Briefly a potential function of the form

$$f(x, y, z) = a_0 + a_1(x - x_0) + a_2(y - y_0) + a_3(z - z_0) \quad (19)$$

is fitted using the potentials ϕ of $N_m (\geq 4)$ nearest grid points in the region of the same dielectric. The coefficients $a_i, (i = 0, 1, 2, 3)$ are determined to minimize

$$d = \sum_m^{N_m} [\phi(x_m, y_m, z_m) - f(x_m, y_m, z_m)]^2 \quad (20)$$

so that the potential and the derivative of potential at position (x_0, y_0, z_0) is given by the following relation:

$$\begin{aligned}
\phi(x_0, y_0, z_0) &\approx f(x_0, y_0, z_0) = a_0 \\
\phi_x(x_0, y_0, z_0) &\approx f_x(x_0, y_0, z_0) = a_1 \\
\phi_y(x_0, y_0, z_0) &\approx f_y(x_0, y_0, z_0) = a_2 \\
\phi_z(x_0, y_0, z_0) &\approx f_z(x_0, y_0, z_0) = a_3
\end{aligned}
\tag{21}$$

Furthermore, the least-square interpolation was conducted without the singular Coulombic field, *i.e.* only the reaction field potential was used in the interpolation. There are two benefits in this choice. (1) The notoriously difficult problem of obtaining accurate surface potential is somewhat alleviated at any finite grid spacing, because the most inaccurate component, the Coulombic field is removed. (2) Coulombic field at the surface is computed analytically. Indeed, the first-order procedure would not be sufficient if Coulombic field is interpolated since the atomic charge is often too close to the surface. This strategy does not incur extra cost since we have to compute the Coulombic interaction between these surface projected polarization charges and atomic charges in the calculation of reaction field energy and forces. Of course, the strategy would be awkward if we have to call the FDM solver twice to compute the reaction field potential. Fortunately our singularity-free formulation for FDM developed recently allows this to be achieved quite efficiently with one FDM call.³¹

D. Surface polarization charge calculation

The surface polarization charges are calculated using the Gauss law and the grid potential obtained from the FDM.²⁹ The boundary grid polarization charges are projected on the molecular surface according to the procedure described by Rocchia *et al.*²⁹

E. Data analysis

An issue important for stable dynamics simulation is the numerical uncertainty of solvation forces when the finite-difference grid is randomly positioned. Sensitivity of grid

positions respect to the solute molecule has been a particularly annoying limitation in current numerical FDM solutions. Here a total of 64 different finite-difference grid origins were used to analyze the numerical uncertainty of different methods, *i.e.* the effect of relative location of finite-difference grids with respect to the interface and charge distribution.

F. Other details

The dielectric interface between the solute and solvent regions was defined by the solvent-excluded molecular surface, obtained with a solvent probe radius 0.6 Å. Note that the unconventionally small probe radius was optimized based on our quantitative comparative analyses of the Poisson-Boltzmann implicit solvent and the TIP3P explicit solvent.⁷² In Ref 72 and subsequent analysis⁷³⁻⁷⁴ we found that the electrostatic solvation energies of small molecules are not very sensitive to the different probe sizes. However, the electrostatic potentials of mean force of hydrogen-bonded or salt-bridge dimers are quite sensitive to the probe radius used and a solvent probe radius of 0.6 Å can best reproduce the TIP3P solvent among the tested probe radii.⁷³⁻⁷⁴ Our subsequent analysis of ion pairs on peptides and proteins also indicates that the probe radius of 0.6 Å can best reproduce the solvation free energies in the TIP3P solvent. Of course, the numerical procedure proposed here works for any other solvent probe. The dielectric constant outside was set as 80.0, and the dielectric constant inside was set as 1.0. The grid spacing was chosen from 1/2 Å to 1/16 Å. The finite-difference convergence criterion was set to be 10^{-9} . All molecular structures were first processed with Leap in AMBER 10⁷⁵ and the modified Bondi radii were used except the radii of all hydrogen atoms were changed to 1.0 Å. No electrostatic focusing was used. The dimension of the grid with respect to the solute was set to be as small as 1.2 to accommodate

the use of the extremely small grid spacing of $1/16 \text{ \AA}$. This is not a problem for our current analysis of *DBF* since our primary focus is on the convergence and numerical uncertainty of the *DBF*. Other parameters were set to be default as in the PBSA program^{15, 28, 31-32} of AMBER 10.⁷³

III. Results and discussion

A. Model systems

We first used a well-studied testing system, a single dielectric sphere imbedded with point charges, to study the validity of eqn (18). The radius of the sphere R is 2.0 \AA , about the size of a united carbon atom, centered at $(0, 0, 0)$. Three typical situations are considered: (a) charged system with a unit positive charge positioned at $(0.5, 0, 0)$; (b) dipolar system with two unit charges located at $(-0.5, 0, 0)$ and $(0.5, 0, 0)$, respectively. (c) quadrupolar system with four unit charges located at $(-0.5, 0.5, 0)$, $(-0.5, -0.5, 0)$, $(0.5, -0.5, 0)$ and $(0.5, 0.5, 0)$.

The *DBF* surface distributions are shown in Figure 1. The analytical distributions are also shown as reference. It is clear that in all three test cases the *DBF* distributions converge to the analytical values as the grid spacing is reduced from $1/2 \text{ \AA}$ to $1/16 \text{ \AA}$. Note too that the *DBF* distributions deviate noticeably from the analytical values at the coarsest grid spacing of $1/2 \text{ \AA}$, and the deviation is reduced as the grid spacing is reduced. More quantitatively the average standard deviations and average root-mean-squared (RMS) deviations (between the mean and the analytical forces) of *DBF* decrease with a factor of 2 – 4, as grid spacing is reduced by half (Table 1). At the same time, the results of Gilson *et al.* are also shown for comparison. It can be seen from Table 1, both methods converge to the analytical values as the grid spacing is reduced to $1/16 \text{ \AA}$, with very similar accuracy, indicating a very high level

of consistency at the finest tested grid spacing. At the coarsest grid spacing of $1/2 \text{ \AA}$ both the average standard deviations and RMS deviations of eqn (18) are better than those of Gilson *et. al*, though the improvements are not very impressive, different from the observation in realistic molecules as will be shown below.

B. Molecular systems

Atomic polarization charges We used two salt-bridging amino acid side chain pairs RD and KD to analyze the convergence of atomic polarization charges. Figure 2 shows the convergence of the mean polarization charge on each atom over reducing grid spacing. It is interesting to note that the mean polarization charges converge well at the grid spacing of $1/2 \text{ \AA}$. Average standard deviations and average deviations (versus the values at $1/16 \text{ \AA}$) of atomic polarization charges are also analyzed and shown in Table 2.

Singularity removal in field interpolation The same salt-bridging side-chain pairs were also used to highlight the importance of the charge singularity removal. Table 3 shows that the standard deviations of computed forces are smaller with singularity removal than those without singularity removal, indicating a more stable algorithm performance. In addition, RMS deviations and correlation coefficients (CC) of forces with respect to the forces computed at the grid spacing of $1/16 \text{ \AA}$ are clearly better with singularity removal than those without singularity removal, indicating faster convergence with respect to the grid spacing.

Atomic dielectric boundary forces We selected additional molecular systems to test the new *DBF* formulation, including two hydrogen-bonding base pairs (CG and AT) and two biopolymers (polyAT and polyALA). As shown in Methods and in analytical model systems, the new formulation is mathematically consistent with that proposed by Gilson *et al*. Here

their consistency is demonstrated by the correlation coefficient (CC) and RMS deviation between the two sets of atomic *DBF*'s. These correlation data are shown in the bold face for the grid spacing of 1/16 Å in Table 4. Overall CC ranges from 0.999299 to 0.999773 and RMS deviation ranges from 0.020 to 0.057 kcal/(mol Å), with RMS relative deviation in the order of 10^{-2} for atomic force magnitudes of at least 3.32 kcal/(mol Å). Finally the standard deviations and RMS deviations decrease by $\sim 2 - 4$ as the grid spacing reduces by half in both methods.

The most apparent advantage of the new method is its much lower numerical uncertainty at coarser grid spacings. It can be seen from Table 4 that the standard deviations of atomic *DBF* by the new method are up to 6 times smaller than those by Gilson *et al.* at the grid spacing of 1/2 Å. At finer grid spacings, the standard deviation by Gilson *et al.* reduces more dramatically: the standard deviation by the new method is about 3 – 4 times smaller than that Gilson *et al.* at the finest grid spacing of 1/16 Å.

The second advantage of the new method is its faster convergence of atomic *DBF* at coarser grid spacings: the RMS deviations of atomic *DBF* at coarser grid spacings with respect to the benchmark data at the grid spacing of 1/16 Å are about 2 to 4 times smaller than those by Gilson *et al.* (Table 4). In addition, CC of the new method with respect to the computed forces at the grid spacing of 1/16 Å ranges from 0.989392 to 0.997477, while that of Gilson *et al.* ranges from 0.914655 to 0.975337. The largest improvement of the new method over Gilson *et al.* is at grid spacing of 1/2 Å as shown in Figure 3, which plots the correlations between atomic *DBF* at 1/2 Å and at 1/16 Å for all tested molecules with both methods. These plots are consistent with the correlation analysis presented in Table 4,

indicating that the new method converges faster than Gilson *et al.* at the coarsest grid spacing of 1/2 Å. Finally, the convergence qualities of the atomic *DBF* for polyAT over different grid spacings are also shown in Figure 4, further indicating that the new method converges faster than Gilson *et al.*

Total electrostatic force An important issue in the force calculation is whether an algorithm leads to energy-conserved molecular dynamics simulations. Often numerical error in force calculation exists so that system dynamics appears under the influence of external force. A good *DBF* formulation should in principle lead to zero total force. Since analytical Coulombic forces are guaranteed to sum up to zero, solvation electrostatic forces, including reaction field forces and *DBF*, should sum up to zero as well. Apparently, it is impossible to guarantee zero total solvation electrostatic force at any finite grid spacing due to the existence of numerical error. Nevertheless, the total force should at least converge to zero as grid spacing is reduced. Table 5 shows that the standard deviations of total electrostatic forces are reduced when the grid spacing is reduced, indicating more accurate total forces at finer grid spacing. The mean total forces also converge to zero as the grid spacing is reduced in both methods, though their convergence is not as impressive as that of the atomic *DBF*. In general, this is a much harder problem, requiring a much higher self-consistency among all related numerical components.

The most significant improvement of the new method over Gilson *et al.* is the much-reduced standard deviations of total forces: reductions in the order of ~ 6 can be observed. This is consistent with the analysis of atomic *DBF*. The reduction in the mean total forces is also noticeable, but not as dramatic as in the standard deviation: mean total forces

four times smaller are often observed at the coarse grid spacings. Note also that the comparative advantage of the new method over Gilson *et al.* is reduced at the finest grid spacing: both standard deviation and the mean become comparative between the two methods. The inaccuracy of *DBF* at coarse grid spacings may result from the direct use of FDM Coulomb potential in Gilson *et al* since the error finally goes away due to the much higher numerical accuracy of Coulomb potential at the finest grid spacing.

Conformation dependence To understand how well the new method and Gilson *et al.* respond to conformation change, we monitored the total electrostatic force on base C of the CG dimer with respect to different base pair distance (Figure 5). Note that the analytical Coulombic forces and numerical reaction field forces are also included to analyze the two methods in the context of total electrostatic interactions. In this analysis the average forces by the new method and Gilson *et al.* at the grid spacing of $1/16 \text{ \AA}$ is used as benchmark. Consistent with our analyses above, the most significant improvement of the new method over Gilson *et al.* is at the coarsest grid spacing of $1/2 \text{ \AA}$: the standard deviations of the total electrostatic forces are reduced significantly by the new method though the deviations of mean total forces from the benchmark are quite similar between the two methods. As the grid spacing reduces, the standard deviations and the deviations from the benchmark both reduces dramatically for both methods. Furthermore, the mean total forces by the two methods become highly consistent when the finest grid spacing is used.

C. “Newton’s Third Law” algorithm

Finally, we tested the previously proposed “Newton’s Third Law” algorithm for the *DBF* calculation. See for example the implementations in Delphi and Amber 10.^{27-29, 75} Similar to

the new formulation developed in this study, this algorithm also utilizes the polarization charges. However, the *DBF* is derived based on the fact that the reaction field force must be balanced to satisfy the Newton’s third law. Here we use the single-charged sphere in section III.A as an example to disprove the algorithm since analytical solution exists for such a simple system. Figure 6 shows the surface distribution of *DBF* for the tested system by the algorithm. The analytical results are also shown as reference. The total *DBF* on the single sphere clearly satisfies the Newton’s third law by design, but the surface distribution is very different from the analytical solution: the algorithm tends to over-estimate the *DBF* density. Thus the agreement between the algorithm and theory for the total *DBF* for the single-charged sphere is merely coincident.

D. Limitations of the new formulation and future directions

As we have discussed in the methods, there are several advantages in the new formulation that utilizes the dielectric boundary charges. When the surface charges are projected to the analytical molecular surface, the grid-dependence in *DBF* can be greatly reduced. However, use of surface charges has a disadvantage, that is, its scaling, in the order of $O(N_{atom} \times N_{bnd})$, is clearly worse than $O(N_{atom}^2)$ because there are always far more dielectric boundary grid points than atoms. Fortunately, the pairwise interaction between the atoms and boundary grid points only needs to be computed once for both the reaction field force and the *DBF*. Nevertheless, the total cost of numerical forces can exceed that of the numerical FDM solution in dynamics simulations if a well-optimized solver is used. This shows that better-scaled methods are still needed.

Another difficulty in the *DBF* calculation comes from the geometric complexity of the

widely used molecular surface definition: *i.e.* there are two types of surface, contact surface from the van der Waals hard sphere surface and reentry surface from the solvent probe. There are two consequences resulted from the complexity. The first consequence is its unsmooth nature, *i.e.* the surface curvature is not always continuous. Indeed, discontinuity always occurs where the contact surface joints the reentry surface. Even more seriously, the curvature does not exist when the reentry surface is reduced to a point in certain geometric arrangements. When numerical integration of DBF is evaluated on such a surface, certain loss of numerical stability can be expected even if the new formulation is used. We are actively working to develop smoother molecular surface definitions that are still highly consistent with the classical molecular surface definition in this group. The geometric complexity also results in the second consequence – there exist two kinds of surface forces: one on the contact region that can be easily translated to the atoms; the other on the reentry region that is hard to be assigned to a particular atom. This is because the DBF is a continuum concept, arising from the existence of two continuum bodies, *i.e.* solvent and solute. In this analysis, we have partitioned the DBF to different atoms in a rather *ad hoc* manner. More physical strategy that considers the very nature of continuum solvent is clearly needed and is under development in this group.

IV. Conclusion

Numerical Poisson-Boltzmann methods have been shown to be successful in a wide range of biomolecular applications, but their applications are quite limited in molecular mechanics simulations, in part, due to the difficulty in the calculation of DBF . In this work, we first review the theory for the DBF calculation based on the Maxwell stress tensor. Then a

new algorithm is developed for the FDM solutions based on the concept of polarization charges. The performance of the new algorithm is then analyzed in detail and compared with a well-established method.

Our analysis shows that the mean polarization charges converge well. We then analyzed the effect of charge singularity removal in the computation of *DBF* and noticed a significant improvement when the charge singularity is removed. We further tested the new *DBF* formulation with multiple small molecules and two biopolymers. The results show that the new formulation is consistent with Gilson *et al.* on the tested molecules. The most apparent advantage of the new method is its much lower numerical uncertainty at coarse grid spacings. The standard deviations of atomic forces by the new method are up to 6 times smaller than that by Gilson *et al.* at the grid spacing of $1/2 \text{ \AA}$. The second advantage of the new method is its faster convergence of atomic forces at coarser grid spacings: the RMS deviations of atomic forces at coarse grid spacings with respect to the benchmark data at the grid spacing of $1/16 \text{ \AA}$ are about 2 to 4 times smaller than those by Gilson *et al.* As far as total electrostatic forces are concerned, the most significant improvement of the new method over Gilson *et al.* is the much-reduced standard deviations: reductions up to 6 times can be observed. This is consistent with the analysis of atomic forces.

Finally, we also tested the previously proposed “Newton’s Third Law” algorithm for the *DBF* calculation. Our analysis shows that even if the total force on the single sphere clearly satisfies the Newton’s third law by design, the surface distribution is very different from analytical solution: the algorithm tends to over-estimate the dielectric force density. Thus, the agreement between the algorithm and theory for the total *DBF* for the single-charged sphere

is merely coincident.

It should be pointed out that the better numerical behavior of the new formulation over that of the Gilson *et al.* comes at a cost, that is, its scaling, in the order of $O(N_{atom} \times N_{bnd})$, is clearly worse than $O(N_{atom}^2)$ because there are always far more dielectric boundary grid points than atoms. Nevertheless, the pair-wise interaction between the atoms and boundary grid points only needs to be computed once for both the reaction field forces and the *DBF*. However, more efforts are clearly needed to develop algorithms that are both stable and efficient.

Acknowledgements

We are grateful for critical reading of the manuscript by Drs. M.K. Gilson, B. Li, and J.A. McCammon, whose comments have led to significantly improvement of the theoretical development and presentation. This work is supported in part by NIH [GM069620 & GM079383].

References

1. Davis, M. E.; McCammon, J. A., Electrostatics in biomolecular structure and dynamics. *Chemical Reviews* **1990**, *90* (3), 509-521.
2. Sharp, K. A., Electrostatic interactions in macromolecules. *Current Opinion in Structural Biology* **1994**, *4* (2), 234-239.
3. Gilson, M. K., Theory of electrostatic interactions in macromolecules. *Current Opinion in Structural Biology* **1995**, *5* (2), 216-223.
4. Honig, B.; Nicholls, A., Classical electrostatics in biology and chemistry. *Science* **1995**, *268* (5214), 1144-1149.
5. Bashford, D.; Case, D. A., Generalized born models of macromolecular solvation effects. *Annual Review Of Physical Chemistry* **2000**, *51*, 129-152.
6. Cramer, C. J.; Truhlar, D. G., Implicit solvation models: Equilibria, structure, spectra, and dynamics. *Chemical Reviews* **1999**, *99* (8), 2161-2200.
7. Roux, B.; Simonson, T., Implicit solvent models. *Biophysical Chemistry* **1999**, *78* (1-2), 1-20.
8. Baker, N. A., Improving implicit solvent simulations: A poisson-centric view. *Current Opinion in Structural Biology* **2005**, *15* (2), 137-143.
9. Chen, J. H.; Im, W. P.; Brooks, C. L., Balancing solvation and intramolecular interactions: Toward a consistent generalized born force field. *Journal of the American Chemical Society* **2006**, *128* (11), 3728-3736.
10. Feig, M.; Chocholousova, J.; Tanizaki, S., Extending the horizon: Towards the efficient modeling of large biomolecular complexes in atomic detail. *Theoretical Chemistry Accounts*

2006, *116* (1-3), 194-205.

11. Im, W.; Chen, J. H.; Brooks, C. L., Peptide and protein folding and conformational equilibria: Theoretical treatment of electrostatics and hydrogen bonding with implicit solvent models. In *Peptide solvation and h-bonds*, Elsevier Academic Press Inc: San Diego, 2006; Vol. 72, pp 173-198.

12. Koehl, P., Electrostatics calculations: Latest methodological advances. *Current Opinion in Structural Biology* **2006**, *16* (2), 142-151.

13. Lu, B. Z.; Zhou, Y. C.; Holst, M. J.; McCammon, J. A., Recent progress in numerical methods for the poisson-boltzmann equation in biophysical applications. *Communications in Computational Physics* **2008**, *3* (5), 973-1009.

14. Wang, J.; Tan, C. H.; Tan, Y. H.; Lu, Q.; Luo, R., Poisson-boltzmann solvents in molecular dynamics simulations. *Communications in Computational Physics* **2008**, *3* (5), 1010-1031.

15. Cai, Q.; Hsieh, M. J.; Wang, J.; Luo, R., Performance of nonlinear finite-difference poisson-boltzmann solvers. *Journal of Chemical Theory and Computation* **2010**, In Press.

16. Klapper, I.; Hagstrom, R.; Fine, R.; Sharp, K.; Honig, B., Focusing of electric fields in the active site of copper-zinc superoxide dismutase effects of ionic strength and amino acid modification. *Proteins Structure Function and Genetics* **1986**, *1* (1), 47-59.

17. Gilson, M. K.; Sharp, K. A.; Honig, B. H., Calculating the electrostatic potential of molecules in solution - method and error assessment. *Journal Of Computational Chemistry* **1988**, *9* (4), 327-335.

18. Davis, M. E.; McCammon, J. A., Solving the finite-difference linearized

poisson-boltzmann equation - a comparison of relaxation and conjugate-gradient methods.

Journal Of Computational Chemistry **1989**, *10* (3), 386-391.

19. Nicholls, A.; Honig, B., A rapid finite-difference algorithm, utilizing successive over-relaxation to solve the poisson-boltzmann equation. *Journal Of Computational Chemistry* **1991**, *12* (4), 435-445.

20. Luty, B. A.; Davis, M. E.; McCammon, J. A., Solving the finite-difference nonlinear poisson-boltzmann equation. *Journal of Computational Chemistry* **1992**, *13* (9), 1114-1118.

21. Holst, M.; Kozack, R. E.; Saied, F.; Subramaniam, S., Protein electrostatics - rapid multigrid-based newton algorithm for solution of the full nonlinear poisson-boltzmann equation. *Journal of Biomolecular Structure & Dynamics* **1994**, *11* (6), 1437-1445.

22. Forsten, K. E.; Kozack, R. E.; Lauffenburger, D. A.; Subramaniam, S., Numerical-solution of the nonlinear poisson-boltzmann equation for a membrane-electrolyte system. *Journal of Physical Chemistry* **1994**, *98* (21), 5580-5586.

23. Holst, M.; Saied, F., Multigrid solution of the poisson-boltzmann equation. *Journal of Computational Chemistry* **1993**, *14* (1), 105-113.

24. Madura, J. D.; Briggs, J. M.; Wade, R. C.; Davis, M. E.; Luty, B. A.; Ilin, A.; Antosiewicz, J.; Gilson, M. K.; Bagheri, B.; Scott, L. R.; McCammon, J. A., Electrostatics and diffusion of molecules in solution - simulations with the university-of-houston brownian dynamics program. *Computer Physics Communications* **1995**, *91* (1-3), 57-95.

25. Bashford, D., An object-oriented programming suite for electrostatic effects in biological molecules. *Lecture Notes in Computer Science* **1997**, *1343*, 233-240.

26. Im, W.; Beglov, D.; Roux, B., Continuum solvation model: Computation of electrostatic

- forces from numerical solutions to the poisson-boltzmann equation. *Computer Physics Communications* **1998**, *111* (1-3), 59-75.
27. Rocchia, W.; Alexov, E.; Honig, B., Extending the applicability of the nonlinear poisson-boltzmann equation: Multiple dielectric constants and multivalent ions. *Journal of Physical Chemistry B* **2001**, *105* (28), 6507-6514.
28. Luo, R.; David, L.; Gilson, M. K., Accelerated poisson-boltzmann calculations for static and dynamic systems. *Journal Of Computational Chemistry* **2002**, *23* (13), 1244-1253.
29. Rocchia, W.; Sridharan, S.; Nicholls, A.; Alexov, E.; Chiabrera, A.; Honig, B., Rapid grid-based construction of the molecular surface and the use of induced surface charge to calculate reaction field energies: Applications to the molecular systems and geometric objects. *Journal of Computational Chemistry* **2002**, *23* (1), 128-137.
30. Wang, J.; Cai, Q.; Li, Z. L.; Zhao, H. K.; Luo, R., Achieving energy conservation in poisson-boltzmann molecular dynamics: Accuracy and precision with finite-difference algorithms. *Chemical Physics Letters* **2009**, *468* (4-6), 112-118.
31. Cai, Q.; Wang, J.; Zhao, H. K.; Luo, R., On removal of charge singularity in poisson-boltzmann equation *Journal of Chemical Physics* **2009**, *130* (14), 145101.
32. Wang, J.; Luo, R., Assessment of linear finite-difference poisson-boltzmann solvers. *Journal of Computational Chemistry* **2010**, *31*, In press.
33. You, T. J.; Harvey, S. C., Finite-element approach to the electrostatics of macromolecules with arbitrary geometries. *Journal of Computational Chemistry* **1993**, *14* (4), 484-501.
34. Cortis, C. M.; Friesner, R. A., Numerical solution of the poisson-boltzmann equation using tetrahedral finite-element meshes. *Journal of Computational Chemistry* **1997**, *18* (13),

1591-1608.

35. Holst, M.; Baker, N.; Wang, F., Adaptive multilevel finite element solution of the poisson-boltzmann equation i. Algorithms and examples. *Journal of Computational Chemistry* **2000**, *21* (15), 1319-1342.
36. Baker, N.; Holst, M.; Wang, F., Adaptive multilevel finite element solution of the poisson-boltzmann equation ii. Refinement at solvent-accessible surfaces in biomolecular systems. *Journal Of Computational Chemistry* **2000**, *21* (15), 1343-1352.
37. Chen, L.; Holst, M. J.; Xu, J. C., The finite element approximation of the nonlinear poisson-boltzmann equation. *Siam Journal on Numerical Analysis* **2007**, *45*, 2298-2320.
38. Shestakov, A. I.; Milovich, J. L.; Noy, A., Solution of the nonlinear poisson-boltzmann equation using pseudo-transient continuation and the finite element method. *Journal of Colloid and Interface Science* **2002**, *247* (1), 62-79.
39. Xie, D.; Zhou, S., A new minimization protocol for solving nonlinear poisson-boltzmann mortar finite element equation. *BIT Numerical Mathematics* **2007**, *47* (4), 853-871.
40. Miertus, S.; Scrocco, E.; Tomasi, J., Electrostatic interaction of a solute with a continuum - a direct utilization of abinitio molecular potentials for the prevision of solvent effects. *Chemical Physics* **1981**, *55* (1), 117-129.
41. Zauhar, R. J.; Morgan, R. S., A new method for computing the macromolecular electric-potential. *Journal of Molecular Biology* **1985**, *186* (4), 815-820.
42. Hoshi, H.; Sakurai, M.; Inoue, Y.; Chujo, R., Medium effects on the molecular electronic-structure .1. The formulation of a theory for the estimation of a molecular electronic-structure surrounded by an anisotropic medium. *Journal of Chemical Physics* **1987**,

87 (2), 1107-1115.

43. Zauhar, R. J.; Morgan, R. S., The rigorous computation of the molecular electric-potential. *Journal of Computational Chemistry* **1988**, *9* (2), 171-187.

44. Juffer, A. H.; Botta, E. F. F.; Vankeulen, B. A. M.; Vanderploeg, A.; Berendsen, H. J. C., The electric-potential of a macromolecule in a solvent - a fundamental approach. *Journal of Computational Physics* **1991**, *97* (1), 144-171.

45. Rashin, A. A., Hydration phenomena, classical electrostatics, and the boundary element method. *Journal of Physical Chemistry* **1990**, *94* (5), 1725-1733.

46. Yoon, B. J.; Lenhoff, A. M., A boundary element method for molecular electrostatics with electrolyte effects. *Journal of Computational Chemistry* **1990**, *11* (9), 1080-1086.

47. Zhou, H. X., Boundary-element solution of macromolecular electrostatics - interaction energy between 2 proteins. *Biophysical Journal* **1993**, *65* (2), 955-963.

48. Bharadwaj, R.; Windemuth, A.; Sridharan, S.; Honig, B.; Nicholls, A., The fast multipole boundary-element method for molecular electrostatics - an optimal approach for large systems. *Journal of Computational Chemistry* **1995**, *16* (7), 898-913.

49. Purisima, E. O.; Nilar, S. H., A simple yet accurate boundary-element method for continuum dielectric calculations. *Journal of Computational Chemistry* **1995**, *16* (6), 681-689.

50. Liang, J.; Subramaniam, S., Computation of molecular electrostatics with boundary element methods. *Biophysical Journal* **1997**, *73* (4), 1830-1841.

51. Vorobjev, Y. N.; Scheraga, H. A., A fast adaptive multigrid boundary element method for macromolecular electrostatic computations in a solvent. *Journal Of Computational Chemistry*

1997, *18* (4), 569-583.

52. Totrov, M.; Abagyan, R., Rapid boundary element solvation electrostatics calculations in folding simulations: Successful folding of a 23-residue peptide. *Biopolymers* **2001**, *60* (2), 124-133.

53. Boschitsch, A. H.; Fenley, M. O.; Zhou, H. X., Fast boundary element method for the linear poisson-boltzmann equation. *Journal of Physical Chemistry B* **2002**, *106* (10), 2741-2754.

54. Lu, B. Z.; Cheng, X. L.; Huang, J. F.; McCammon, J. A., Order n algorithm for computation of electrostatic interactions in biomolecular systems. *Proceedings of the National Academy of Sciences of the United States of America* **2006**, *103* (51), 19314-19319.

55. Davis, M. E.; McCammon, J. A., Calculating electrostatic forces from grid-calculated potentials. *Journal of Computational Chemistry* **1990**, *11* (3), 401-409.

56. Zauhar, R. J., The incorporation of hydration forces determined by continuum electrostatics into molecular mechanics simulations. *Journal of Computational Chemistry* **1991**, *12* (5), 575-583.

57. Sharp, K., Incorporating solvent and ion screening into molecular-dynamics using the finite-difference poisson-boltzmann method. *Journal of Computational Chemistry* **1991**, *12* (4), 454-468.

58. Niedermeier, C.; Schulten, K., Molecular-dynamics simulations in heterogeneous dielectrics and debye-huckel media - application to the protein bovine pancreatic trypsin-inhibitor. *Molecular Simulation* **1992**, *8* (6), 361-387.

59. Gilson, M. K.; Davis, M. E.; Luty, B. A.; McCammon, J. A., Computation of electrostatic

forces on solvated molecules using the poisson-boltzmann equation. *Journal of Physical Chemistry* **1993**, *97* (14), 3591-3600.

60. Friedrichs, M.; Zhou, R. H.; Edinger, S. R.; Friesner, R. A., Poisson-boltzmann analytical gradients for molecular modeling calculations. *Journal of Physical Chemistry B* **1999**, *103* (16), 3057-3061.

61. Grant, J. A.; Pickup, B. T.; Nicholls, A., A smooth permittivity function for poisson-boltzmann solvation methods. *Journal Of Computational Chemistry* **2001**, *22* (6), 608-640.

62. Che, J.; Dzubiella, J.; Li, B.; McCammon, J. A., Electrostatic free energy and its variations in implicit solvent models. *Journal of Physical Chemistry B* **2008**, *112* (10), 3058-3069.

63. Lu, B. Z.; McCammon, J. A., Improved boundary element methods for poisson-boltzmann electrostatic potential and force calculations. *Journal of Chemical Theory and Computation* **2007**, *3* (3), 1134-1142.

64. Lu, B. Z.; Zhang, D. Q.; McCammon, J. A., Computation of electrostatic forces between solvated molecules determined by the poisson-boltzmann equation using a boundary element method. *Journal of Chemical Physics* **2005**, *122* (21), 7.

65. Rashin, A. A., Electrostatics of ion ion interactions in solution. *Journal of Physical Chemistry* **1989**, *93* (11), 4664-4669.

66. Vorobjev, Y. N.; Grant, J. A.; Scheraga, H. A., A combined iterative and boundary element approach for solution of the nonlinear poisson-boltzmann equation. *Journal of the American Chemical Society* **1992**, *114* (9), 3189-3196.

67. Yoon, B. J.; Lenhoff, A. M., Computation of the electrostatic interaction energy between a protein and a charged surface. *Journal of Physical Chemistry* **1992**, *96* (7), 3130-3134.
68. Lu, Q.; Luo, R., A poisson-boltzmann dynamics method with nonperiodic boundary condition. *Journal of Chemical Physics* **2003**, *119* (21), 11035-11047.
69. Landau, L. D.; Lifshitz, E. M.; Pitaevskii, L. P., *Electrodynamics of continuous media* (pergamon press,oxford, 1984)
70. Sharp, K. A.; Honig, B., Calculating total electrostatic energies with the nonlinear poisson-boltzmann equation. *Journal of Physical Chemistry* **1990**, *94* (19), 7684-7692.
71. Li, Z.; Ito, K., *The Immersed Interface Method: Numerical Solutions of PDEs Involving Interfaces and Irregular Domains*, SIAM Society for Industrial and Applied Mathematics, Philadelphia, 2006.
72. Tan, C. H.; Yang, L. J.; Luo, R., How well does poisson-boltzmann implicit solvent agree with explicit solvent? A quantitative analysis. *Journal of Physical Chemistry B* **2006**, *110* (37), 18680-18687.
73. Wang, J.; Tan, C. H.; Chanco, E.; Luo, R., Accuracy and limitation of poisson-boltzmann implicit solvent in molecular dynamics simulations. *Physical Chemistry Chemical Physics* (*in press*).
74. Ye, X.; Cai, Q.; Yang, W.; Luo, R., Roles of boundary conditions in DNA simulations: Analysis of ion distributions with the finite-difference poisson-boltzmann method. *Biophysical Journal* **2009**, *97* (2), 554-562.
75. Case, D. A.; Cheatham, T. E.; Darden, T.; Gohlke, H.; Luo, R.; Merz, K. M.; Onufriev, A.;

Simmerling, C.; Wang, B.; Woods, R. J., The amber biomolecular simulation programs.

Journal of Computational Chemistry **2005**, 26 (16), 1668-1688.

Tables

Table 1. Convergence of dielectric boundary forces (kcal/(mol Å)) in the spherical analytical systems. σ and $rmsd$ are, respectively, the average standard deviations of dielectric boundary forces and average root mean squared deviations of dielectric boundary forces from analytical values. Both σ and $rmsd$ are computed over the 30 bins used to divide the spherical surface. See Figure 1 for more details.

	1/h	This work		Gilson <i>et al.</i> ⁵⁹	
		σ	$rmsd$	σ	$rmsd$
single-charged	2	.515	.065	.614	.109
	4	.151	.028	.169	.037
	8	.083	.011	.070	.008
	16	.022	.005	.023	.003
dipolar-charged	2	.325	.086	.372	.110
	4	.099	.015	.100	.021
	8	.042	.007	.047	.006
	16	.014	.004	.014	.002
quadrupolar-charged	2	.408	.123	.551	.153
	4	.141	.059	.161	.030
	8	.058	.032	.062	.011
	16	.019	.016	.019	.003

Table 2. Convergence and uncertainty of atomic polarization charges (e) for salt-bridged amino acid side chain dimers RD and KD. σ and $rmsd$ are, respectively, the average standard deviations of atomic polarization charges and the average root mean squared deviations of atomic polarization charges from those computed with the finest tested grid spacing.

	1/h	$\sigma (\times 10^{-3})$	$rmsd (\times 10^{-3})$
RD	2	2.74	2.28
	4	1.02	1.45
	8	.379	.659
	16	.142	NA
KD	2	3.30	1.69
	4	1.20	.794
	8	.473	.501
	16	.168	NA

Table 3. Convergence and uncertainty of atomic dielectric boundary forces (kcal/(mol Å)) for salt-bridge amino acid side chain dimers RD and KD with and without singularity removal. σ and *rmsd* are, respectively, the average standard deviations of atomic dielectric boundary forces and the average root mean squared deviations of atomic dielectric boundary forces from those computed with the finest tested grid spacing.

		w/o singularity			with singularity		
	1/h	CC	<i>rmsd</i>	σ	CC	<i>rmsd</i>	σ
RD	2	.995702	.207	.109	.991407	1.05	.307
	4	.999824	.063	.034	.998444	.382	.053
	8	.999959	.024	.013	.999851	.110	.016
	16	N/A	N/A	.005	N/A	N/A	.006
KD	2	.995221	.205	.091	.992494	1.26	.243
	4	.999585	.080	.035	.998621	.395	.051
	8	.999917	.028	.014	.999871	.117	.017
	16	N/A	N/A	.006	N/A	N/A	.007

Table 4. Convergence and uncertainty of atomic dielectric boundary forces (kcal/(mol Å)) for several selected molecular systems. CC: correlation coefficient with the atomic dielectric boundary forces computed with the finest tested grid spacing. σ and *rmsd* are defined in Table 3. Note that the numbers in bold are between “This work” and “Gilson *et al.*⁵⁹”.

		This work (no singularity)			Gilson <i>et al.</i> ⁵⁹		
	1/h	CC	<i>rmsd</i>	σ	CC	<i>rmsd</i>	σ
CG	2	.989392	.251	.123	.914655	.737	.765
	4	.998643	.089	.053	.988039	.232	.216
	8	.999837	.030	.023	.998173	.087	.080
	16	.999299	.057	.009	N/A	N/A	.030
AT	2	.995179	.118	.083	.944397	.345	.414
	4	.999587	.048	.023	.994972	.085	.112
	8	.999965	.018	.009	.999585	.024	.037
	16	.999763	.023	.003	N/A	N/A	.013
polyAT	2	.997477	.141	.071	.973263	.378	.394
	4	.999670	.054	.027	.996563	.119	.124
	8	.999958	.019	.010	.999699	.034	.043
	16	.999773	.032	.004	N/A	N/A	.015
polyALA	2	.995408	.069	.030	.975337	.208	.193
	4	.999462	.031	.013	.997356	.056	.063
	8	.999949	.011	.005	.999516	.020	.022
	16	.999773	.020	.003	N/A	N/A	.008

Table 5. Convergence and uncertainty of total electrostatic forces (kcal/(mol Å)) for several selected molecular systems. σ and *mean* are, respectively, standard deviations and means of total electrostatic forces for the tested systems.

	1/h	This work		Gilson <i>et al.</i> ⁵⁹	
		<i>mean</i>	σ	<i>mean</i>	σ
CG	2	3.30	1.98	13.7	13.9
	4	2.76	.398	11.0	3.39
	8	2.08	.115	5.84	1.02
	16	1.78	.038	2.90	.435
AT	2	1.51	1.21	4.91	5.58
	4	.614	.195	2.89	1.43
	8	.471	.063	1.81	.627
	16	.432	.025	1.32	.262
RD	2	1.52	1.28	8.33	9.69
	4	.727	.335	2.37	4.02
	8	.687	.076	3.14	2.13
	16	.651	.030	1.49	.525
KD	2	.823	1.41	2.75	7.87
	4	.594	.274	2.08	5.05
	8	.548	.093	1.23	1.87
	16	.535	.031	.369	.392
polyAT	2	12.0	4.05	26.4	22.5
	4	6.94	.747	16.3	5.91
	8	5.71	.234	7.54	2.49
	16	5.51	.095	5.64	.850
polyALA	2	3.29	1.01	5.64	7.60
	4	2.21	.282	3.95	3.08
	8	1.87	.084	3.39	.930
	16	1.71	.032	3.06	.425

Figures

Figure 1. Convergence of dielectric boundary forces (magnitude, in kcal/(mol Å)) on a sphere in the single-charged arrangement (top), dipolar-charged arrangement (middle), and quadrupolar-charged arrangement (bottom), respectively. Left: this work. Right: Gilson *et al.*⁵⁹ The spherical surface is divided into 30 bins. Theta is the inclination angle from the zenith for each bin. The analytical results are shown as solid black lines. The detailed statistics of the tests are listed in Table 1.

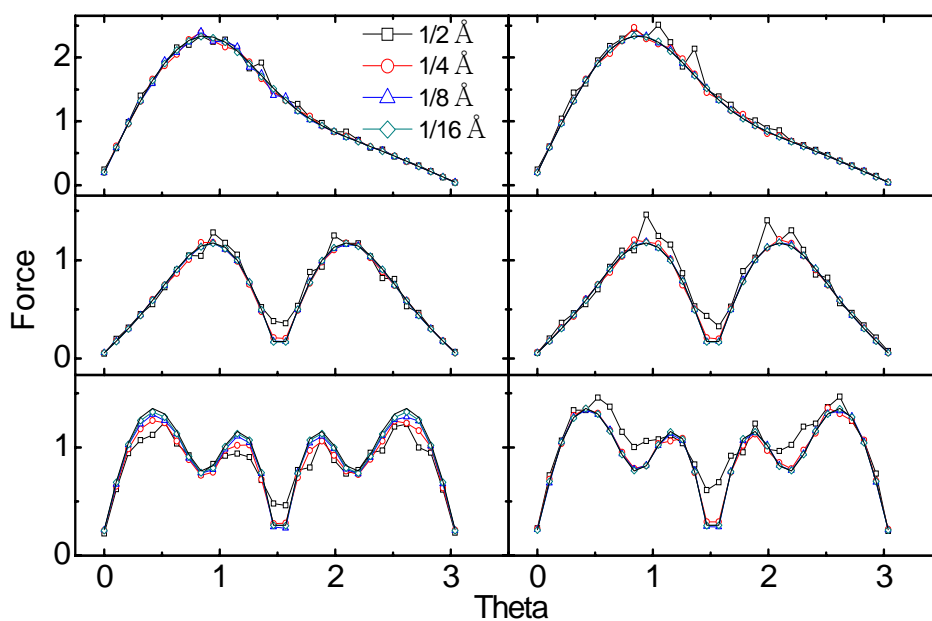


Figure 2. Convergence of atomic polarization charges (e) of dimer RD (top) and KD

(bottom).

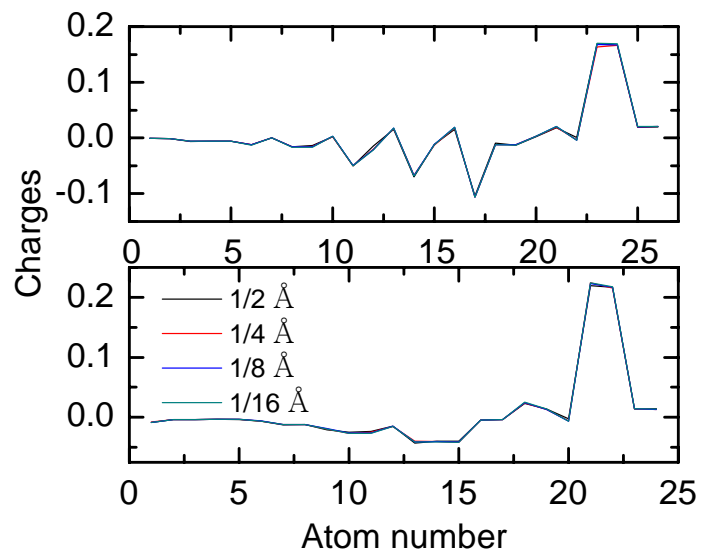


Figure 3. Correlations between the atomic dielectric boundary forces (kcal/(mol Å)) computed at the 1/2 Å grid spacing and those at the 1/16 Å grid spacing. Results from this work are shown in cyan open square, and results from Gilson *et al.*⁵⁹ are shown in magenta open triangle. Top: two base pairs and two side chain pairs. Middle: polyALA. Bottom: polyAT.

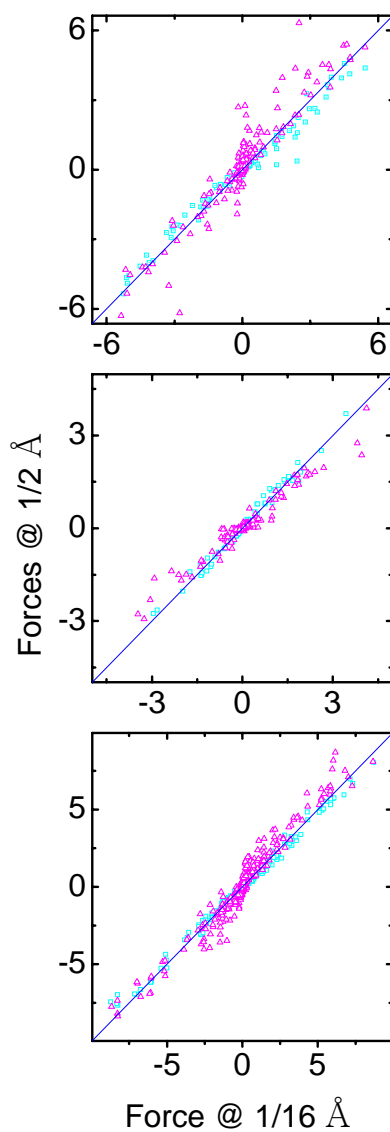


Figure 4. Correlations between atomic dielectric boundary forces (kcal/(mol Å)) computed at the grid spacings of 1/2 Å, 1/4 Å, and 1/8 Å, respectively, and those at the grid spacing of 1/16 Å for polyAT. Left: This work. Right: Gilson *et al.*⁵⁹

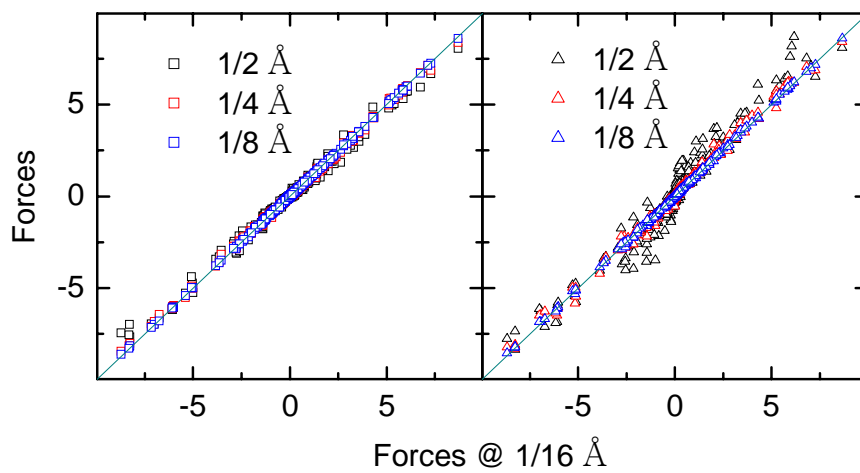


Figure 5. Total electrostatic force (kcal/(mol Å)) on base C of the CG dimer with respect to inter-molecular distance (Å, between atoms N3 on C and H1 on G). The results of this work are shown in cyan triangle, the results of Gilson *et al.* are shown in magenta square, and the average data of 1/16 Å by both methods are used as the benchmark, shown in blue circle. Note that the standard deviations in Gilson *et al.*⁵⁹ are out of the plotting range at 1/2 Å.

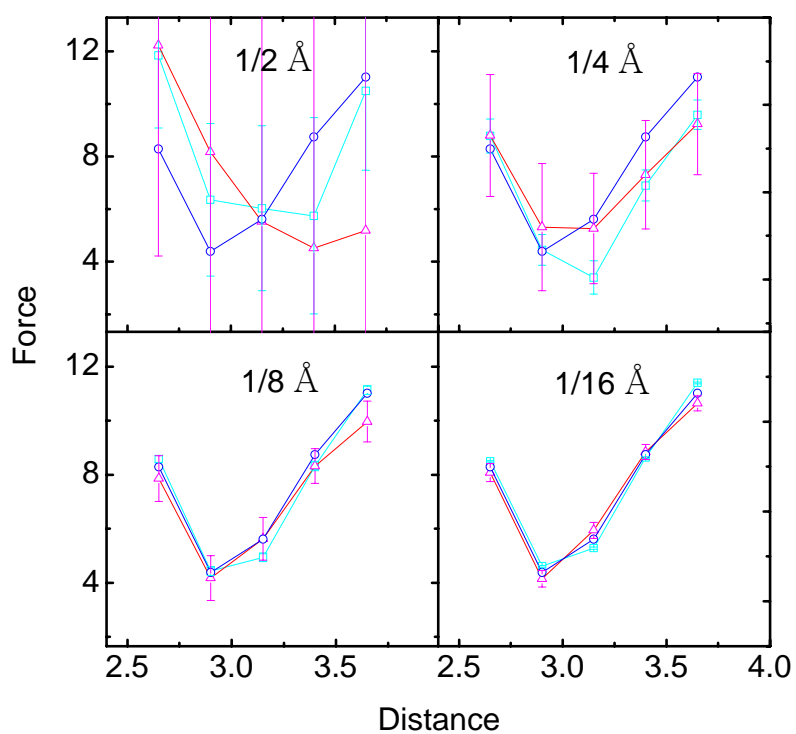


Figure 6. Dielectric boundary forces (kcal/(mol Å)) on a single-charged sphere by the “Newton’s third law” algorithm. Analytical results are also shown for comparison. See Figure 1 for more detail. Here X is the force in the x direction; Z is for the force in the z direction. The force in the y direction is extreme small, and is not shown.

